

Microstrain and defects in polycrystalline $\text{Zn}_{1-x}\text{Mg}_x\text{O}$ ($0 \leq x \leq 0.15$) studied by X-ray diffraction, and optical and Raman spectroscopies

Young-Il Kim and Ram Seshadri

*Materials Department and Materials Research Laboratory,
University of California, Santa Barbara, California 93106, USA*

(Dated: Received April 18, 2022)

The properties of polycrystalline wurtzite $\text{Zn}_{1-x}\text{Mg}_x\text{O}$ ($0 \leq x \leq 0.15$) have been studied, by powder X-ray diffraction, including an analysis of the X-ray line-broadening, and by luminescence, absorption, and Raman spectroscopies. We have previously established from synchrotron X-ray diffraction that with increasing Mg-concentration, the c -axis compresses, and the off-center cation displacement within each tetrahedral $(\text{Zn,Mg})\text{O}_4$ unit decreases. Here we perform a size-strain line-broadening analysis of the XRD peaks, which reveals that the Mg-substitution reduces the coherent crystallite size and also develops the lattice microstrain. The optical properties of the samples have been characterized by diffuse-reflectance spectroscopy and fluorimetry. Both the optical band gap and the band-edge emission energies gradually increase with the Mg-concentration in $\text{Zn}_{1-x}\text{Mg}_x\text{O}$. The Mg-substituted samples show broader band tails near the absorption edge, due to the increase of crystal imperfections. The peak broadening of the E_2^{high} Raman mode, upon the Mg-substitution, is also ascribed to the phonon shortening lifetime mechanism *via* crystal defects.

PACS numbers: 61.10.Nz, 71.55.Gs, 77.22.Ej

Keywords: ZnO, $\text{Zn}_{1-x}\text{Mg}_x\text{O}$, polar semiconductor, X-ray line-broadening, photoluminescence, Raman

I. INTRODUCTION

Zinc oxide (ZnO) is well known for the diverse uses deriving from semiconducting, piezoelectric, pyroelectric, photoluminescent, and photocatalytic characteristics.[1, 2, 3] Among other properties, the polar crystal lattice of ZnO provides great potential for developing two-dimensional electron gas (2DEG) *via* the construction of heterojunction structures. A 2DEG can be created at heterojunction interface that bears a polarization gradient, with both high carrier concentration and high carrier mobility.[4] In the recent experiments on II-VI or III-V semiconductors, 2DEG have been well utilized for exploring novel transistor devices[5, 6] as well as the quantum Hall effect[7].

The alloy $\text{Zn}_{1-x}\text{Mg}_x\text{O}$ is a suitable system for exploiting the ZnO-based 2DEG, since the Mg-substitution provides an efficient way to tune the polarization strength of ZnO crystal with only minimal changes of lattice dimensions.[8] The polarization in $\text{Zn}_{1-x}\text{Mg}_x\text{O}$ and the 2DEG quality of ZnO/ $\text{Zn}_{1-x}\text{Mg}_x\text{O}$ heterostructure will depend mostly on the crystal structure details of $\text{Zn}_{1-x}\text{Mg}_x\text{O}$ alloy. Hence the sensible design of ZnO/ $\text{Zn}_{1-x}\text{Mg}_x\text{O}$ heterostructure devices requires a comprehensive knowledge of structural evolutions across $\text{Zn}_{1-x}\text{Mg}_x\text{O}$ solid solutions.

The composition-dependent structure evolution of $\text{Zn}_{1-x}\text{Mg}_x\text{O}$ alloy using synchrotron X-ray diffraction has been presented by us previously.[8, 9] The use of high-flux and high-energy synchrotron radiation enabled us to trace small changes of wurtzite parameters (a , c , and u) in $\text{Zn}_{1-x}\text{Mg}_x\text{O}$ solid solutions. In addition line-broadening analysis[10, 11, 12] of powder XRD patterns provides information on the crystallite morphology and Mg patterns in $\text{Zn}_{1-x}\text{Mg}_x\text{O}$ phases. The XRD analyses show that the Mg substitution modifies the macroscopic distortion of the hexagonal lattice through the enhanced bond ionicity, and also that the static polarization in the crystal can be gradually

varied, in parallel with the internal tetrahedral distortion, as a function of Mg content. The effects of Mg-substitution on the optical properties and Raman spectra are also discussed here. Raman spectroscopy, which is known to be a powerful probe of compositional disorder and/or the strain within semiconductor alloys,[13, 14] corroborates the findings from XRD analyses.

II. EXPERIMENTS

Polycrystalline $\text{Zn}_{1-x}\text{Mg}_x\text{O}$ ($x = 0, 0.05, 0.10, 0.15$ and 0.20) samples were prepared by an oxalate co-precipitation way.[8, 9] Zinc acetate and magnesium acetate were dissolved together in deionized water in the stoichiometric cation ratios, and mixed with separately prepared oxalic acid solution. The resulting precipitates were thoroughly washed and dried at 60°C for 4 h to produce white and crystalline $\text{Zn}_{1-x}\text{Mg}_x(\text{C}_2\text{O}_4) \cdot 2\text{H}_2\text{O}$ powders. The oxalate dihydrates were converted to the oxides $\text{Zn}_{1-x}\text{Mg}_x\text{O}$ by heating in air at 550°C for 24 h. Powder X-ray diffraction (XRD) identified the phase pure $\text{Zn}_{1-x}\text{Mg}_x(\text{C}_2\text{O}_4) \cdot 2\text{H}_2\text{O}$ and $\text{Zn}_{1-x}\text{Mg}_x\text{O}$ after the heating steps of 60°C and 550°C , respectively. Thermogravimetry of $\text{Zn}_{1-x}\text{Mg}_x(\text{C}_2\text{O}_4) \cdot 2\text{H}_2\text{O}$, in air up to 1000°C , confirmed that the oxide $\text{Zn}_{1-x}\text{Mg}_x\text{O}$ phases are formed through well-defined processes of dehydration and the oxalate decomposition.

For the crystal structure determinations by Rietveld analysis, synchrotron XRD patterns of $\text{Zn}_{1-x}\text{Mg}_x\text{O}$ were measured on beamline 11-ID-B of the Advanced Photon Source (Argonne National Laboratory, USA) with an X-ray wavelength of 0.13648 \AA . The XRD patterns for the line-broadening analysis were obtained using an in-house X-ray diffractometer (Philips X'PERT MPD, $\text{Cu } K\alpha_{1,2}$). Instrumental broadening was corrected using the data measured for LaB_6 (grain size $\approx 10 \mu\text{m}$). Diffuse-reflectance absorption spectra

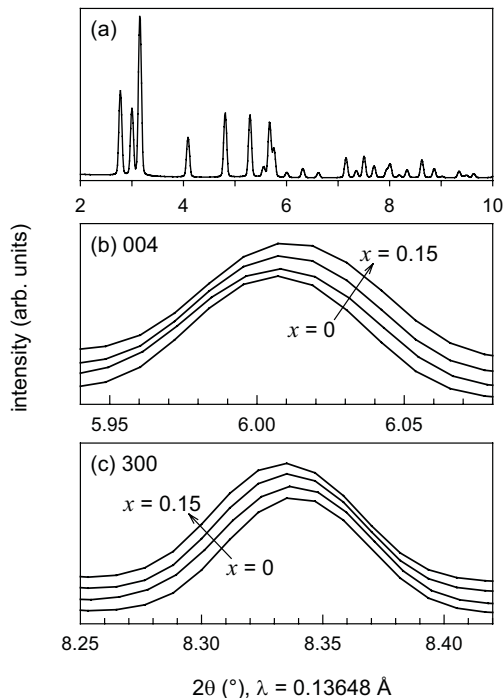


FIG. 1: (a) Synchrotron XRD pattern for ZnO and the zoomed views of (b) in-plane 004 and (c) out-of-plane 300 XRD peaks for $\text{Zn}_{1-x}\text{Mg}_x\text{O}$ ($x = 0, 0.05, 0.10,$ and 0.15).

were recorded for $\text{Zn}_{1-x}\text{Mg}_x\text{O}$ in the wavelength range of 220–800 nm using a Shimadzu UV-3600 spectrophotometer equipped with an ISR-3100 integrating sphere. The optical band gap was determined by extrapolating the linear part of the absorption edge to zero-absorption level. Photoluminescence of $\text{Zn}_{1-x}\text{Mg}_x\text{O}$ powders were studied using a Perkin-Elmer LS55 luminescence spectrometer at room temperature. Emission spectra were recorded employing an excitation wavelength of 340 nm. Raman spectra at room temperature were acquired using an optical microprobe fitted with a single monochromator (Jobin-Yvon, T64000). An Ar^+ laser ($\lambda = 488$ nm) excitation was used with a beam power of 50 mW and a spot size of ≈ 2 μm . The E_2^{high} phonon mode was used for detailed peak profile analyses. The background was removed following Shirley[15], and Breit-Wigner-Fano type peak fitting[16] was carried out to determine peak position and the width.

III. RESULTS AND DISCUSSION

The synchrotron XRD pattern for ZnO is shown in Figure 1a, which is consistent with the wurtzite-type hexagonal structure. All the Mg-substituted phases ($x = 0.05, 0.10, 0.15,$ and 0.20) presented nearly indistinguishable XRD patterns to that of ZnO, but the $x = 0.20$ phase was found to contain cubic MgO as a secondary phase. Therefore the solubility of Mg in $\text{Zn}_{1-x}\text{Mg}_x\text{O}$ is estimated to be slightly higher than 15 %, under the preparational conditions employed here. The ionic radii of

TABLE I: Crystallite size and strain of $\text{Zn}_{1-x}\text{Mg}_x\text{O}$ powders as determined by the size-strain line-broadening analysis using the simplified integral-breadth method.

x	D_v (nm)	D_a (nm)	ϵ (%)
0	96(3)	69(3)	<0.01
0.05	76(3)	57(3)	0.020(6)
0.10	70(2)	51(3)	0.028(5)
0.15	62(2)	47(2)	0.041(4)
0.20	33(1)	27(1)	0.099(7)

D_v : volume-weighted crystallite size.
 D_a : surface area-weighted crystallite size.
 ϵ : strain averaged over the distance $D_v/2$.

4-coordinate Mg^{2+} (0.57 Å) and Zn^{2+} (0.60 Å) are similar[17] but the two cations will demand distinct extents of geometric distortions in the tetrahedral environment. The resulting structural evolution in $\text{Zn}_{1-x}\text{Mg}_x\text{O}$ solid solutions can be first recognized from the peak positions of $00l$ and $h00$ reflections. As displayed in Figure 1b and c, the 004 and 300 diffraction peaks of $\text{Zn}_{1-x}\text{Mg}_x\text{O}$ are shifted to higher and lower angles, respectively, as x increases. Namely, the hexagonal lattice constant a increases and c decreases with the progress of Mg-substitution in ZnO.

For the quantitative determinations of structural parameters, Rietveld refinements were performed for $\text{Zn}_{1-x}\text{Mg}_x\text{O}$ using a structure model based on wurtzite ZnO; space group $P6_3mc$, Zn/Mg at $(\frac{1}{3}, \frac{2}{3}, 0)$ and O at $(\frac{1}{3}, \frac{2}{3}, u)$. [8] Rietveld refinements confirmed that the wurtzite structure is retained for all the $\text{Zn}_{1-x}\text{Mg}_x\text{O}$ phases studied here, and also that the Mg-substitution in ZnO accompanies the expansion of ab -dimension, compression of c -dimension, and consequently the decrease of c/a ratio. The a and c parameters follow approximately, the relationships: $a(\text{Å}) = 3.2503 + 0.0118x$ and $c(\text{Å}) = 5.2072 - 0.0232x$, as functions of x . The variations of a , c , and c/a in $\text{Zn}_{1-x}\text{Mg}_x\text{O}$ solid solutions are consistent with the general trend found in the binary wurtzite family, that is, c/a ratio becomes smaller as the bonding character becomes more ionic.[18] It is the increased ionicity that Mg^{2+} provides in $\text{Zn}_{1-x}\text{Mg}_x\text{O}$ which results in the c -axis compression of the hexagonal lattice.

The internal tetrahedral distortion and the spontaneous polarization in $\text{Zn}_{1-x}\text{Mg}_x\text{O}$ can be assessed using the atomic position parameter u . The four nearest cation-anion pairs are equidistant if $u = \frac{1}{3}(\frac{a}{c})^2 + \frac{1}{4}$, whereas the charge separation in each tetrahedral unit will vanish if $u = \frac{3}{8}$. The Rietveld-refined u monotonously decreased from 0.3829 for ZnO to 0.3819 for $\text{Zn}_{0.85}\text{Mg}_{0.15}\text{O}$. [8] This indicates that the tetrahedral distortion in ZnO is gradually relieved by alloying with MgO, and that ionic polarization of $\text{Zn}_{1-x}\text{Mg}_x\text{O}$ should decrease with the Mg concentration. This was also supported by pair-distribution-function studies of $\text{Zn}_{1-x}\text{Mg}_x\text{O}$. [9]

In order to examine the effect of Mg-substitution on the microstructure and crystallite morphology, XRD line-broadening analysis was performed for $\text{Zn}_{1-x}\text{Mg}_x\text{O}$ ($x = 0, 0.05, 0.10, 0.15$ and 0.20). As noted ahead the sample with $x = 0.20$ showed an indication of MgO segregation, which

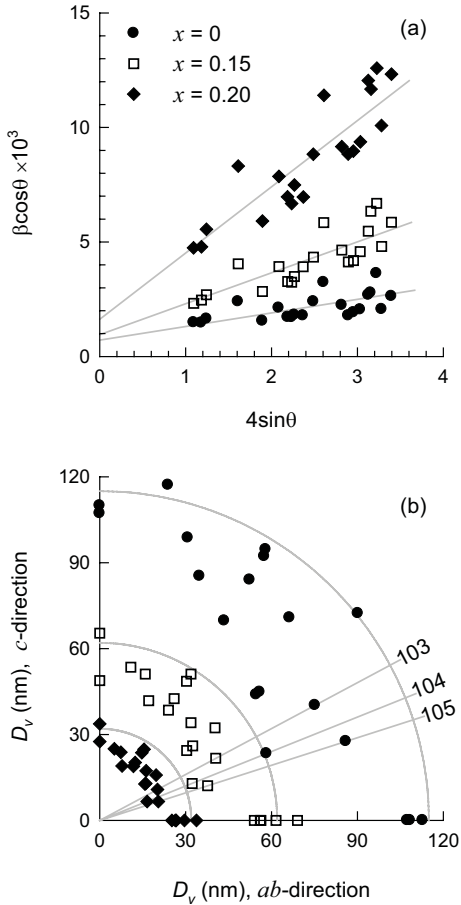


FIG. 2: (a) Williamson-Hall plots and (b) polar diagrams of apparent crystallite size D_v for $Zn_{1-x}Mg_xO$ with $x = 0, 0.15$, and 0.20 .

implies that the remaining wurtzite phase is nearly saturated with Mg. The line-broadening data for $x = 0.20$ can therefore be taken as the morphological characteristics at the solubility limit. The integral-breadth (β) of each peak was calculated using the full-width-at-half-maximum and the shape factor m of split-Pearson VII function, with an aid of the software BREADTH[12].

Figure 2 shows the Williamson-Hall (W-H) plots[19] for the three samples of $x = 0, 0.15$, and 0.20 , together with the polar diagrams of crystallite size. The W-H plot is based on the following function,

$$\beta_i \cos \theta_i = \frac{\lambda}{D_v} + 4\epsilon \sin \theta_i \quad (1)$$

where β_i is the integral-breadth (in radians 2θ) of the i th Bragg reflection positioned at $2\theta_i$. The slope and the ordinate intercept of the W-H plot can be used to quantify crystallite size (D_v) and strain(ϵ) contributions to peak broadening.

In Figure 2a, the data points on each W-H plot are more or less scattered around a mean straight line. A close investigation of ZnO data revealed that the $00l$ or $h00$ type peak groups have much narrower widths than the $h0l$ ones. In fact, the uniaxial ($00l$, $h00$) and the off-axial ($h0l$) diffraction

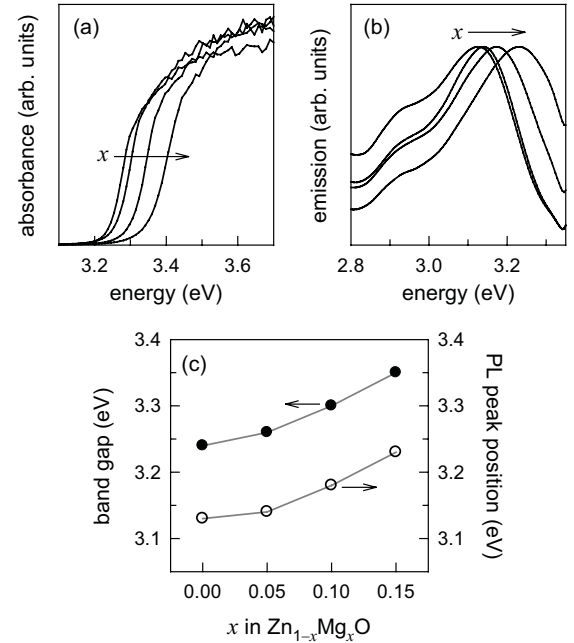


FIG. 3: Optical properties of polycrystalline $Zn_{1-x}Mg_xO$ ($x = 0, 0.05, 0.10$ and 0.15) measured at $20^\circ C$, (a) diffuse-reflection absorption, (b) photoluminescence excited at 340 nm (3.65 eV), and (c) band gap and photoluminescence peak energies as functions of Mg content.

peak groups fall on their own straight lines. They have different slopes but nearly the same intercept, implying that the ZnO crystallites are reasonably isotropic, but have considerable amount of stacking faults. The polar diagrams in Figure 2b displays the crystallite dimensions along different crystallographic directions. In common for the three samples, D_v is largest along the $h00$, $hk0$ or $00l$ -directions, and becomes smaller in the hkl and $h0l$ directions. Particularly, the $10l$ peaks showed pronounced peak broadening. However, there is found no significant anisotropic line-broadening caused by the Mg-substitution, indicating that the Mg is distributed in $Zn_{1-x}Mg_xO$ in a random manner.

Table I lists the crystallite sizes and microstrain evaluated by using BREADTH. Mg-substitution in ZnO decreases the XRD-coherent crystallite size and at the same time introduces greater microstrain. The Zn/Mg exchange itself will affect the periodicity of the atomic arrangement and also induces various types of structural defects and microstrain as well. This will be important in the following consideration of optical properties.

Figure 3 shows the absorption and photoluminescence spectra of $Zn_{1-x}Mg_xO$ powders, measured at room temperature. Clearly, both the band gap (E_g) transition (Figure 3a) and the band-edge emission (Figure 3b) are blue-shifted as the Mg content increases in the $Zn_{1-x}Mg_xO$. Although the solid solution of MgO–ZnO only involves isovalent substitution, the electronic structure of ZnO is substantially modified by the incorporation of Mg. The conduction band of wurtzite ZnO is mainly contributed from the Zn $4s$ orbital. However in the $Zn_{1-x}Mg_xO$, the Mg $3s$ orbitals contribute as well. Since the

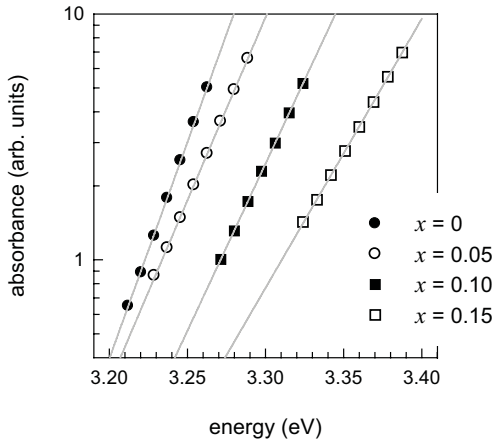


FIG. 4: Semilogarithmic plots $\text{Log } A$ vs. $h\nu$ near the band-edge for $\text{Zn}_{1-x}\text{Mg}_x\text{O}$, $x = 0, 0.05, 0.10,$ and 0.15 .

$\text{Mg } 3s$ orbital lies at a higher energy level than the $\text{Zn } 4s$, the Mg -substitution in ZnO will move the conduction band-edge upward, thereby widening the band gap.

In order to evaluate the near band-edge characteristics of the $\text{Zn}_{1-x}\text{Mg}_x\text{O}$ powders, we used a description by Pankove[20] of the absorbance (A) in the near band-edge region:

$$A \propto \exp \frac{h\nu}{E_0} \quad (2)$$

where E_0 is an empirical parameter having dimensions of energy and describing the width of the localized states in the band gap but not their energy position. It can be regarded that E_0 accounts for the effects of all possible defects (point, line, and planar dislocations). In Figure 4 are shown the absorbance of $\text{Zn}_{1-x}\text{Mg}_x\text{O}$ powders as functions of the incident photon energy in the near-edge region. For all the compositions the absorbance shows the expected exponential dependence in the near band-edge regime. It is also observed that the value E_0 increases with x . As determined from the slope of linear fit, the E_0 widths are 24.7 ($x = 0$), 29.2 ($x = 0.05$), 31.9 ($x = 0.10$), and 39.7 meV ($x = 0.15$). Such a change in band tail points out the role of Mg as the defect centers in the $\text{Zn}_{1-x}\text{Mg}_x\text{O}$ lattice. Not surprisingly the long range crystallinity of ZnO lattice will be disturbed in the course of cation substitution, by the creation of point defects, dislocations, impurities, and grain boundaries.

The E_2^{high} Raman mode of $\text{Zn}_{1-x}\text{Mg}_x\text{O}$ powders were analyzed by peak profile analyses. In all cases of $x = 0-0.15$, the E_2^{high} peaks of $\text{Zn}_{1-x}\text{Mg}_x\text{O}$ are best represented by the Breit-Wigner-Fano (BWF) lineshape[16], which is of Lorentzian type, but having the asymmetry character. As shown in Figure 5, each Raman line can be successfully fit to a single BWF component, using the parameters of energy position (ω_0), full-width-at-half-maximum (Γ), BWF coupling coefficient (asymmetry term), and the maximum peak intensity.

As given on Figure 5, the ω_0 and Γ of the $\text{Zn}_{1-x}\text{Mg}_x\text{O}$ E_2^{high} mode systematically change with the Mg -concentration. The redshift of the E_2^{high} mode can be interpreted as the phonon

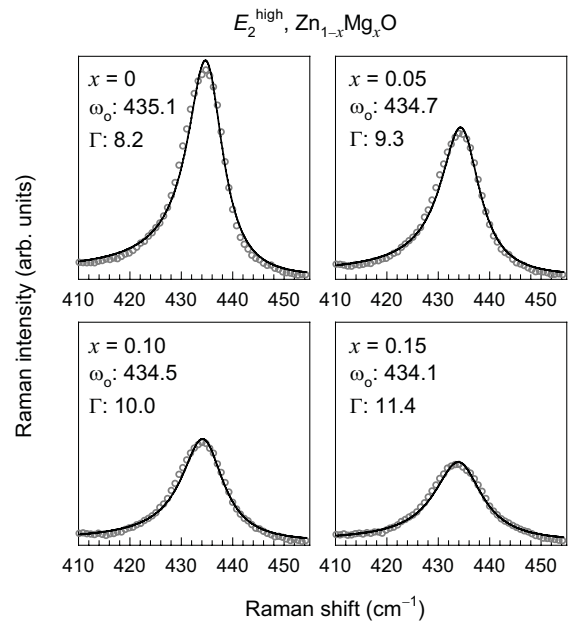


FIG. 5: Profile shape fittings of E_2^{high} Raman peaks for $\text{Zn}_{1-x}\text{Mg}_x\text{O}$ using the Breit-Wigner-Fano function (experimental: circles, fit: line, fit parameters are in cm^{-1}). Same intensity scale is used for all the four panels.

softening *via* expansion of hexagonal *ab*-dimensions.[9] On the other hand, the broadening of the E_2^{high} mode can be understood in a similar context as for the XRD line-broadening and the near-edge absorption behavior. The crystal defects provide common mechanisms for the phonon lifetime (τ) shortening, and are closely related to the Raman linewidth. The energy-time uncertainty relation, $\Gamma/\hbar = 1/\tau$, indicates an inverse linear relationship between Γ and τ . The wider Γ can be attributed to the shorter τ and in turn to the higher defect concentration in the system. Therefore the lineshape of Raman E_2^{high} mode evidences again the increase of crystal defects upon the Mg -substitution in ZnO .

IV. CONCLUSIONS

The average and local crystal structural aspects of $\text{Zn}_{1-x}\text{Mg}_x\text{O}$ were studied by XRD methods using polycrystalline samples. The composition-dependent evolutions of c/a ratio and u parameters are indicative of the polarization gradient along the $\text{Zn}_{1-x}\text{Mg}_x\text{O}$ solid solutions. It is inferred from the XRD line-broadening analysis, that the Mg atoms are homogeneously distributed over the wurtzite $\text{Zn}_{1-x}\text{Mg}_x\text{O}$ lattice without any ordering behavior. Raman spectroscopy provides additional evidences of *a*-lattice expansion upon the Mg -substitution and of the random Mg/Zn distributions. Although the $\text{Zn}_{1-x}\text{Mg}_x\text{O}$ solid solutions are obtained by an isovalent substitution, the band gap varies remarkably with the Mg content. The absorption edge slopes indicate that Mg acts as defect center near the band-edge.

Acknowledgments

Authors thank support from the U.S. National Science Foundation through the MRSEC program (DMR05-20415). Work at Argonne National Laboratory and the Advanced Pho-

ton Source was supported by the U.S. Department of Energy, Office of Science, Office of Basic Energy Sciences, under Contract No. DE-AC02-06CH11357. Authors thank Katharine Page for the synchrotron data collection, and David Clarke for the help in Raman measurement.

-
- [1] U. Ozgur, Ya. I. Alivov, C. Liu, A. Teke, M. A. Reshchikov, S. Dogan, V. Avrutin, S.-J. Cho, and H. Morkoc, *J. Appl. Phys.* **98**, 041301 (2005).
- [2] S. J. Pearton, D. P. Norton, K. Ip, Y. W. Heo, and T. Steiner, *J. Vac. Sci. Tech. B* **22**, 932 (2004).
- [3] D. C. Look, *J. Electron. Mater.* **35**, 1299 (2006).
- [4] J. H. Davies, *The Physics of Low-Dimensional Semiconductors: An Introduction* (Cambridge University Press, New York, 1998).
- [5] H. Tampo, H. Shibata, K. Matsubara, A. Yamada, P. Fons, S. Niki, M. Yamagata, and H. Kanie, *Appl. Phys. Lett.* **89**, 132113 (2006).
- [6] S. Rajan, H. Xing, S. DenBaars, U. K. Mishra, and D. Jena, *Appl. Phys. Lett.* **84**, 1591 (2004).
- [7] A. Tsukazaki, A. Ohtomo, T. Kita, Y. Ohno, H. Ohno, and M. Kawasaki, *Science* **315**, 1388 (2007).
- [8] Y.-I. Kim, K. Page, and R. Seshadri, *Appl. Phys. Lett.* **90**, 101904 (2007).
- [9] Y.-I. Kim, K. Page, A. M. Limarga, D. R. Clarke, and R. Seshadri, *Phys. Rev. B*, in press (2007).
- [10] P. Scardi, M. Leoni, and R. Delhez, *J. Appl. Crystallogr.* **37**, 381 (2004).
- [11] J. I. Langford, D. Louer, E. J. Sonneveld, and J. W. Visser, *Powder Diff.* **1**, 211 (1986).
- [12] D. Balzar, *J. Appl. Cryst.* **28**, 244 (1995).
- [13] H. Richter, Z. P. Wang, and L. Ley, *Solid State Commun.* **39**, 615 (1981).
- [14] K. K. Tiong, P. M. Amirtharaj, F. H. Pollak, and D. E. Aspnes, *Appl. Phys. Lett.* **44**, 122 (1983).
- [15] D. A. Shirley, *Phys. Rev. B* **5**, 4709 (1972).
- [16] M. Yoshikawa, *Mater. Sci. Forum* **52-53**, 365 (1989).
- [17] R. D. Shannon, *Acta Crystallogr. A* **32**, 751 (1976).
- [18] H. Schulz and K. H. Thiemann, *Solid State Commun.* **23**, 815 (1977).
- [19] G. K. Williamson and W. H. Hall, *Acta Metallurgica*, **1**, 22 (1953).
- [20] J. I. Pankove, *Phys. Rev.* **140**, A2059 (1965).